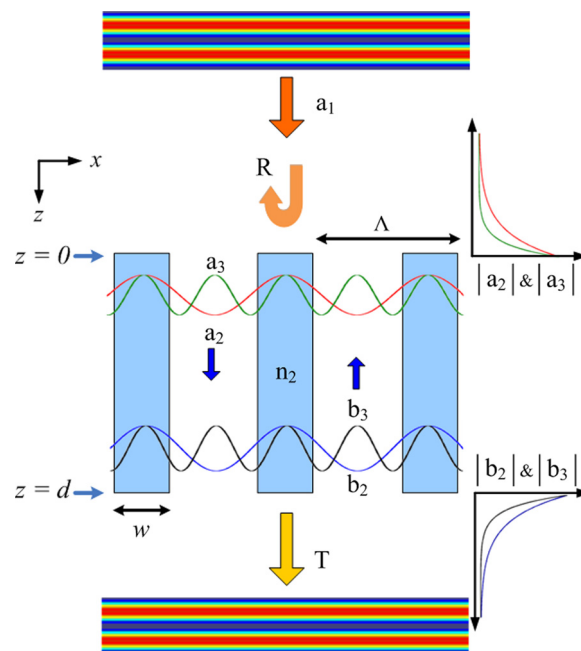


Design and Analysis of High-Index-Contrast Gratings Using Coupled Mode Theory

Volume 2, Number 6, December 2010

Aftab Ahmed
Marco Liscidini
Reuven Gordon, Senior Member, IEEE



DOI: 10.1109/JPHOT.2010.2079322
1943-0655/\$26.00 ©2010 IEEE

Design and Analysis of High-Index-Contrast Gratings Using Coupled Mode Theory

Aftab Ahmed,¹ Marco Liscidini,² and Reuven Gordon,² *Senior Member, IEEE*

¹Department of Electrical and Computer Engineering, University of Victoria,
Victoria, BC V8W 3P6, Canada

²Department of Physics "A. Volta," University of Pavia, 27100 Pavia, Italy

DOI: 10.1109/JPHOT.2010.2079322
1943-0655/\$26.00 ©2010 IEEE

Manuscript received July 28, 2010; revised September 13, 2010; accepted September 14, 2010.
Date of publication September 16, 2010; date of current version October 1, 2010. Corresponding
author: R. Gordon (e-mail: rgordon@uvic.ca).

Abstract: We analyze high-refractive-index-contrast subwavelength grating structures using truncated coupled mode theory (CMT). CMT not only provides physical insight into the role of each mode in the overall response but also allows for improved design. An analytic expression is derived for the design of broadband reflectors, providing a near-optimal design that is within 0.08% of the maximum broadband reflectivity calculated by the finite-difference time-domain method. Furthermore, the CMT is used to design a high-quality narrow-band reflector with 28% improved quality factor over previously reported results, as quantified by rigorous coupled wave analysis.

Index Terms: Photonic materials and engineered photonic structures, theory and design, engineered photonic nanostructures, subwavelength structures.

1. Introduction

Coupled mode theory (CMT) has been widely used for analysis of guiding structures in the optical regime for predicting the effects of periodic perturbations (periodic in the longitudinal/transverse directions) in an otherwise perfect guide [1]. Since its first introduction in early 1950s for microwave devices [2], CMT has experienced a long series of developments, and by the early 1970s, it was applied to optical devices [3], [4]. The method is rigorous if all modes are included. CMT can yield extremely accurate results even if a small subset of the modes is retained; however, CMT can be more efficient than other methods, such as rigorous coupled wave analysis (RCWA) or the finite difference time domain (FDTD), by selecting the appropriate modal expansion. Furthermore, CMT is not limited to periodic boundaries and can be applied quite generally; for example, recently, the perfectly matched layer (PML) has been introduced into the formalism of CMT to simulate an unbounded geometry by discretizing continuous radiation modes while having negligible effect on the bound guided modes [5].

Optical diffraction gratings have been studied for years for their applications in filtering, spectroscopy [6]–[8], lasers, and other optoelectronic devices [9], [10]. Recently, these structures have been employed for bio-sensing applications as well [11]. Gratings with period smaller than the incident wavelength are referred to as subwavelength gratings, and as a result, all higher order modes are evanescently bound, which leads to interesting effects. Typical applications include reflectors for vertical cavity surface emitting lasers (VCSELs) [12]–[14], high-efficiency light-emitting diodes [15], and ultra broadband mirrors [16]. High-index-contrast gratings (HCGs), which are also known as suspended gratings, differ from the conventional subwavelength gratings by the fact that the grating structure is surrounded by a low index material. The HCG was first proposed in 2004

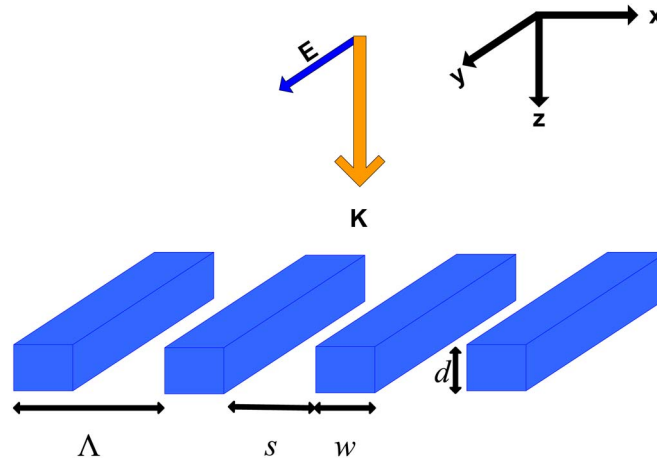


Fig. 1. High-Index Contrast Grating (HCG) with period Λ , width w , thickness d , and spacing s . Incident electric field is parallel to the grating (TE).

[16], [17] and since then has attracted attention for the development of broadband high-reflectivity mirrors due to the high index contrast in the in-plane direction. In the past, numerical methods such as RCWA [18] and the FDTD method [19] have been used to analyze such structures; however, those methods can be computationally taxing and do not provide the physical insight of CMT.

In this paper, we present a CMT approach for the design and analysis of HCGs to achieve close-to-optimal dimensions for a specific application and to understand the underlying physics as it relates to the coupling between optical modes. For the HCG problem, while CMT mode selection provides only a modest reduction in expansion order over RCWA, the CMT method allows for clear insight into the physics of the HCG operation in different parameter regimes, as well as efficient design of near-optimal structures. For the HCG examples considered here, CMT provides accurate results for as few as three modes, showing that these modes indeed have a dominant role in the response of the system. In Section 2, we present the HCG structure and describe the CMT method. Section 3 presents the results and discussions. First, the constraint on coupling coefficients to yield broadband response is derived, and the results obtained are compared with FDTD and RCWA simulations. Second, high-quality (Q) resonators are considered in order to maximize the Q-factor by the adjustment of parameters, and the results are compared with RCWA.

2. CMT Formulation

Fig. 1 shows the HCG structure to be analyzed, the structure is periodic in the x -direction, and the three parameters that dictate the reflectivity of the grating are period (Λ), width (w), and thickness (d). The ratio of width (w) to period (Λ) is defined as the duty cycle (η). The periodic structure is assumed to be surrounded by a homogeneous low index material with refractive index (n_1), whereas the refractive index of the grating is (n_2). The polarization of incident excitation is taken to be transverse electric (TE) with respect to the xz -plane.

The coupled mode equations governing the mode amplitudes are given as (from [5])

$$N_m \left(\frac{da_m}{dz} + j\beta_m a_m \right) = -j \sum_{n=1}^M \kappa_{mn} a_n - j \sum_{n=1}^M \chi_{mn} b_n \quad (1a)$$

$$N_m \left(\frac{db_m}{dz} - j\beta_m b_m \right) = j \sum_{n=1}^M \chi_{mn} a_n + j \sum_{n=1}^M \kappa_{mn} b_n \quad (1b)$$

where a_m and b_m are the mode amplitudes of forward and backward traveling modes, respectively, β_m is the propagation constant, and κ_{mn} and χ_{mn} are the coupling coefficients between co-directional

and contra-directional propagating waves, respectively. These are defined as

$$\kappa_{mn} = \frac{\omega \varepsilon_o}{4} \iint (\tilde{n}^2 - n^2) \left(\mathbf{e}_{tm} \cdot \mathbf{e}_{tn} - \frac{n^2}{\tilde{n}^2} \mathbf{e}_{zm} \cdot \mathbf{e}_{zn} \right) dx dy \quad (2a)$$

$$\chi_{mn} = \frac{\omega \varepsilon_o}{4} \iint (\tilde{n}^2 - n^2) \left(\mathbf{e}_{tm} \cdot \mathbf{e}_{tn} + \frac{n^2}{\tilde{n}^2} \mathbf{e}_{zm} \cdot \mathbf{e}_{zn} \right) dx dy \quad (2b)$$

$$\kappa_{mn} = \kappa_{nm}. \quad (3)$$

In the case of TE polarization

$$\kappa_{mn} = \chi_{mn}. \quad (4)$$

Finally, the normalization constants N_m are defined as

$$N_m = \frac{1}{2} \iint (\mathbf{e}_{tm} \times \mathbf{e}_{tn}) dx dy \quad (5)$$

where ω is the angular frequency of the incident excitation, ε_o is the permittivity of free space, n and \tilde{n} are the refractive indices of the unperturbed and perturbed structures under investigation, respectively, and \mathbf{e}_{tm} and \mathbf{e}_{zm} are the transverse and longitudinal components of the m th mode, respectively.

Due to the periodic nature of the problem, the chosen modes bare close resemblance to the Fourier modes found in RCWA, and the choice of a cosine wave expansion (motivated by the symmetry within the period) does not provide significant reduction in the modes used. Therefore, in this case, as a pure computational method, CMT is not better than RCWA for the HCG problem; however, as we will show in the following analysis, CMT provides additional physical insight into the HCG operation in terms of mode coupling and analytic design criteria can be advised with this approach.

In the following analysis, we consider only three modes ($M = 3$): the fundamental excitation (plane wave with amplitude a_1) and the first two evanescent higher order modes (cosine waves with amplitudes a_2 and a_3). The coupling equations are given as

$$[X]' = [A] \times [X] \quad (6a)$$

where ' signifies differentiation with respect to z , and

$$[X] = [a_1 \ a_2 \ a_3 \ b_1 \ b_2 \ b_3]^T \quad (6b)$$

$$[A] = j \begin{bmatrix} -K_{11} - \beta_1 & -K_{12} & -K_{13} & -\Psi_{11} & -\Psi_{12} & -\Psi_{13} \\ -K_{21} & -K_{22} - \beta_2 & -K_{23} & -\Psi_{21} & -\Psi_{22} & -\Psi_{23} \\ -K_{31} & -K_{32} & -K_{33} - \beta_3 & -\Psi_{31} & -\Psi_{32} & -\Psi_{33} \\ \Psi_{11} & \Psi_{12} & \Psi_{13} & K_{11} + \beta_1 & K_{12} & K_{13} \\ \Psi_{21} & \Psi_{22} & \Psi_{23} & K_{21} & K_{22} + \beta_2 & K_{23} \\ \Psi_{31} & \Psi_{32} & \Psi_{33} & K_{31} & K_{32} & K_{33} + \beta_3 \end{bmatrix} \quad (6c)$$

where $K_{mn} = \kappa_{mn}/N_m$, and $\Psi_{mn} = \chi_{mn}/N_m$. We define all these variables in terms of the dimensions of grating and the incident wavelength, and after performing the required integrations, we obtain

$$K_{11} = \beta_1 q \quad (7a)$$

$$K_{12} = K_{11} \text{sinc}(\pi w/\Lambda) \quad (7b)$$

$$K_{13} = K_{11} \text{sinc}(2\pi w/\Lambda) \quad (7c)$$

$$K_{21} = 2 \frac{\beta_1}{\beta_2} K_{11} \text{sinc}(\pi w/\Lambda) \quad (7d)$$

$$K_{22} = \frac{\beta_1}{\beta_2} K_{11} (1 + \text{sinc}(2\pi w/\Lambda)) \quad (7e)$$

$$K_{23} = \frac{\beta_1}{\beta_2} K_{11} (\text{sinc}(\pi w/\Lambda) + \text{sinc}(3\pi w/\Lambda)) \quad (7f)$$

$$K_{31} = 2 \frac{\beta_1}{\beta_3} K_{11} \text{sinc}(2\pi w/\Lambda) \quad (7g)$$

$$K_{32} = \frac{\beta_1}{\beta_3} K_{11} (\text{sinc}(\pi w/\Lambda) + \text{sinc}(3\pi w/\Lambda)) \quad (7h)$$

$$K_{33} = \frac{\beta_1}{\beta_3} K_{11} (1 + \text{sinc}(4\pi w/\Lambda)) \quad (7i)$$

where q and propagation constants are defined as

$$q = \frac{(n_2^2 - n_1^2) w}{2\Lambda} \quad (8a)$$

$$\beta_1 = \frac{2\pi}{\lambda_o} \quad (8b)$$

$$\beta_2 = \beta_1 \sqrt{1 - \left(\frac{\lambda_o}{\Lambda}\right)^2} \quad (8c)$$

$$\beta_3 = \beta_1 \sqrt{1 - \left(\frac{2\lambda_o}{\Lambda}\right)^2}. \quad (8d)$$

Equation (6) is a system of coupled first-order differential equations; it merely represents an eigenvalue problem, and the solution is given as

$$[X] = [e^{\lambda_a z} V_a \quad e^{\lambda_b z} V_b \quad e^{\lambda_c z} V_c \quad e^{\lambda_d z} V_d \quad e^{\lambda_e z} V_e \quad e^{\lambda_f z} V_f] \times [C] \quad (9a)$$

$$[C] = [c_1 \quad c_2 \quad c_3 \quad c_4 \quad c_5 \quad c_6]^T \quad (9b)$$

where elements of C are the unknown coefficients that need to be determined from the boundary conditions, λ_i are eigenvalues, and V_i are the corresponding eigenvectors. We need six boundary conditions to solve the system of (9). The structure is excited with a forward propagating plane wave only, with amplitude $a_1 = 1$ at $z = 0$; thus, the backward propagating plane wave b_1 has an amplitude of 0 at $z = d$. The remaining boundary conditions are dictated by the possibility of existence of the evanescent waves. Evanescent waves a_2 and a_3 are exponentially increasing with respect to z ; therefore, these must have zero amplitudes at $z = d$ and similar constraints apply to b_2 and b_3 at the $z = 0$ boundary. Application of these boundary conditions results in

$$[C] = F^{-1} \times [1 \quad 0 \quad 0 \quad 0 \quad 0 \quad 0]^T \quad (10a)$$

where

$$[F] = \begin{bmatrix} V_{a1} & V_{b1} & V_{c1} & V_{d1} & V_{e1} & V_{f1} \\ e^{\lambda_a d} V_{a2} & e^{\lambda_b d} V_{b2} & e^{\lambda_c d} V_{c2} & e^{\lambda_d d} V_{d2} & e^{\lambda_e d} V_{e2} & e^{\lambda_f d} V_{f2} \\ e^{\lambda_a d} V_{a3} & e^{\lambda_b d} V_{b3} & e^{\lambda_c d} V_{c3} & e^{\lambda_d d} V_{d3} & e^{\lambda_e d} V_{e3} & e^{\lambda_f d} V_{f3} \\ e^{\lambda_a d} V_{a4} & e^{\lambda_b d} V_{b4} & e^{\lambda_c d} V_{c4} & e^{\lambda_d d} V_{d4} & e^{\lambda_e d} V_{e4} & e^{\lambda_f d} V_{f4} \\ V_{a5} & V_{b5} & V_{c5} & V_{d5} & V_{e5} & V_{f5} \\ V_{a6} & V_{b6} & V_{c6} & V_{d6} & V_{e6} & V_{f6} \end{bmatrix} \quad (10b)$$

where V_{jn} is the n th element of j th eigenvector.

It is interesting to note that at a specific wavelength and dimensions of the gratings, F is nearly singular; this is the condition that results in exponential rise of C , and thus, we observe huge field enhancement of the higher order modes, as will be shown in the results.

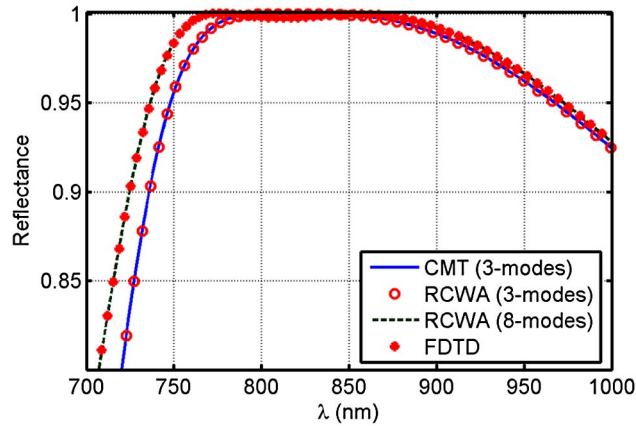


Fig. 2. HCG designed to operate as surface-normal broadband mirror at wavelength of 850 nm, period $\Lambda = 620$ nm, width $w = 220$ nm, and thickness $d = 140$ nm. Reflectivity using the CMT and RCWA with only three lowest order modes, along with fully converged RCWA (8-modes) and FDTD.

3. Results and Discussions

We analyzed HCG for two different applications, namely (a) broadband mirrors and (b) high-Q resonators. Comparisons with RCWA [20] and FDTD verify that this approach produces accurate and insightful results.

3.1. HCG for Surface-Normal Broadband Mirrors

We first demonstrate the accuracy of the results obtained by using CMT with only three lowest order modes. Fig. 2 shows the reflectivity of HCG designed to operate at a wavelength of 850 nm at normal incidence. The grating is comprised of rectangular strips of AlGaAs with refractive index of 3.2 surrounded by air. The dimensions of the grating are period $\Lambda = 620$ nm, width $w = 220$ nm, and thickness $d = 140$ nm. The reflectivity spectra obtained using RCWA and FDTD are also plotted in Fig. 2 for comparison. It should be noted that CMT and RCWA give exactly the same results when equal numbers of modes are used; therefore, the results presented using RCWA are equivalent to that of CMT results (fully converged for eight modes). The advantages of using CMT with few modes are the ability to visualize the mode amplitudes as a function of distance along the propagation direction and the understanding of their interaction with each other. While RCWA matches FDTD, the CMT response is slightly shifted toward longer wavelengths. Nevertheless, it should be noted that although the result is obtained using only three modes, it is in good agreement with those of RCWA and FDTD.

One of the advantages of a CMT approach is the possibility of an analytic design for broadband applications. To derive the necessary conditions for broadband response, we rewrite matrix A of (6c) but for the case of $M = 2$ as

$$A = j \begin{bmatrix} D & E \\ -E & -D \end{bmatrix} \quad (11)$$

where D and E are 2×2 matrices representing the coupling between co-directional and contra-directional propagating modes. For broadband response, we look for the condition when the absolute difference between co-directional coupling and contra-directional coupling changes slightly over the band of operation; therefore, the required condition is $|D| = |E|$. Since the off-diagonal elements cancel, we have

$$(K_{11} + \beta_1)(K_{22} + \beta_2) = K_{11}K_{22}. \quad (12)$$

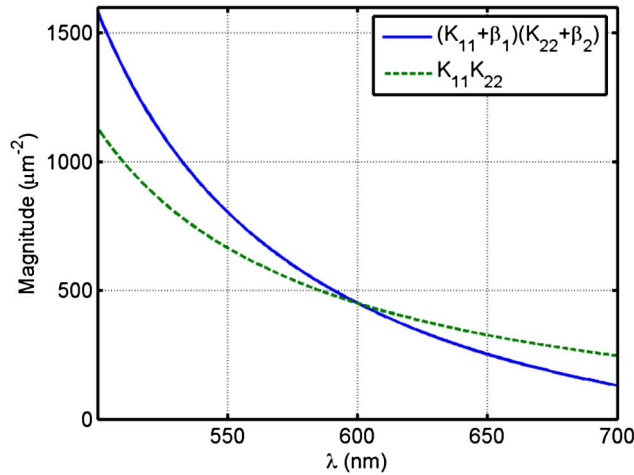


Fig. 3. Same mode co-directional (blue solid line) and contra-directional (green dashed line) coupling as a function of wavelength for the determination of broadband response. Parameters are $\Lambda = 443$ nm, $w = 160.8$ nm, $d = 99$ nm, and $n_2 = 3.2$.

Therefore, when the product of self-coupling approaches the product of coupling coefficients of the same but contra-directional propagating modes, then broadband response is observed. Fig. 3 shows a plot of (12) designed to operate at wavelength of 600 nm; it is this small difference around the center wavelength that causes the broadband response. Equation (12) leads us to the following condition for broadband operation:

$$\beta_2^2 = \frac{-q}{(1+q)} \beta_1^2 \left(1 + \text{sinc} \left(\frac{2\pi w}{\Lambda} \right) \right). \quad (13)$$

For a specific grating index and wavelength of interest, (13) can provide the required period Λ and duty cycle η . Fig. 4(a) shows the points satisfying (13) for a grating index of 3.2 designed to operate at a wavelength of 600 nm. Once the period and width are determined from (13), the next step is the determination of grating thickness d . It should be noted that the design rule of (13) is not just for broadband high reflectivity. It can also be used for the design of broadband high transmittance structures, depending on the thickness d . With the dimensions obtained from Fig. 4(a), we can calculate the required grating thickness resulting in a minimum transmitted power through the grating, which corresponds to the zeros of the fundamental mode a_1 at $z = d$. Fig. 4(b) shows the mode amplitude of the forward propagating mode a_1 at $z = d$ as a function of thickness, dictating the thickness to be 99 nm ($d = 138$ nm will result in broadband high transmittance). Our proposed design guideline provides following dimensions for design A with center wavelength of $\lambda = 600$ nm, $\Lambda = 443$ nm, $w = 160.8$ nm, and $d = 99$ nm. Fig. 4(d) shows mode amplitudes as a function of distance along the propagation direction z of the incident excitation.

To investigate the accuracy of the design procedure, comprehensive numerical simulations using FDTD method were carried out. (FDTD was used here because it is efficient for broadband calculations; however, a few calculations were selected and showed agreement with RCWA.) A comparison of the results obtained using CMT and FDTD methods is shown in Fig. 4(c). FDTD verifies the broadband characteristic of the design. For design criteria of reflectivity higher than 99% over the entire band of operation, FDTD results show that the width w can range from 153 nm to 178 nm. It is noted that the value of 160.8 nm predicted by the proposed design rule falls within this range. Furthermore, it is also observed from FDTD results that the minimum ripple in reflectance is achieved for $w = 167$ nm, resulting in reflectance value of higher than 99.48%, whereas Design A gives a reflectance higher than 99.4% over the entire bandwidth. This confirms that in this case, this design approach provides near-optimal results in terms of ripple. Achieving a large reflection over the band of operation is desired for many applications, such as VCSELs [12]–[14].

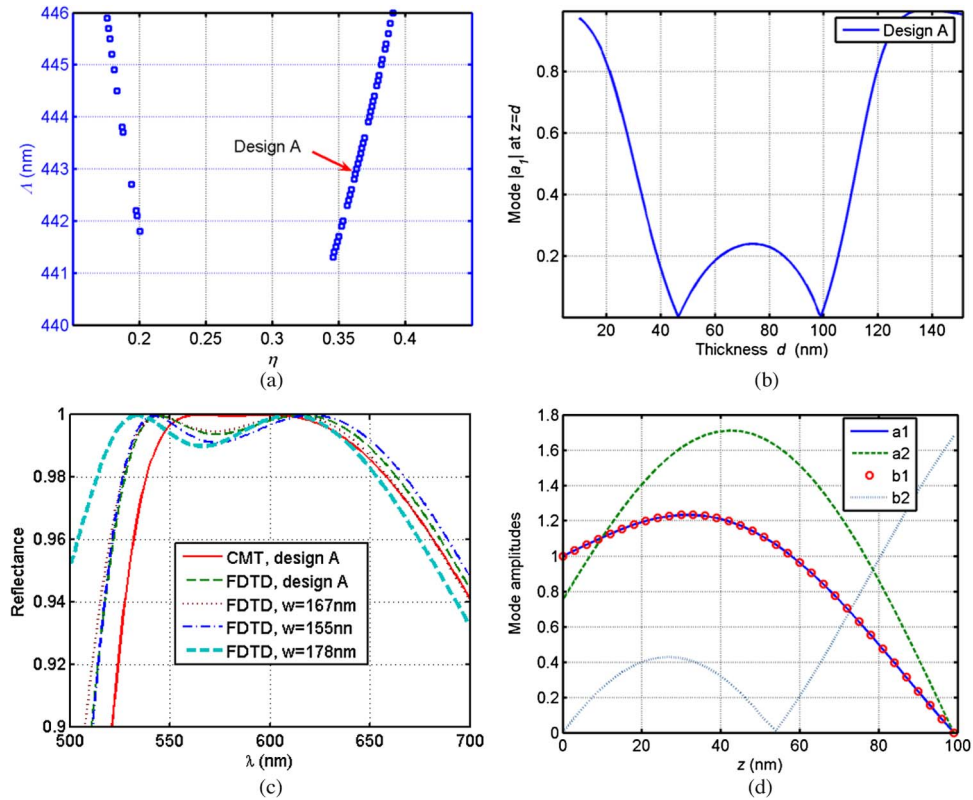


Fig. 4. (a) Design of broadband reflector for center wavelength of 600 nm, with grating index of 3.2. (b) Forward propagating fundamental mode amplitude at $z = d$ for the determination of the optimal thickness. (c) Reflectivity obtained using CMT and FDTD for design A and for slight variations in width. Dimensions for design A are $\Lambda = 443$ nm, $w = 160.8$ nm, and $d = 99$ nm. (d) Mode amplitudes as a function of distance along the propagation direction z of the incident excitation.

3.2. HCG for High-Q Resonators

Another interesting application of HCG is its use as a very narrow-band reflector or high-Q resonator. Precise adjustment of the dimensions can lead to the condition that the average energy in the forward going mode is completely coupled into the backward propagating modes at the opposite interface of structure over a very narrow band of frequencies. This condition is achieved when the matrix F given by (10b) becomes nearly singular, which is approached when any two rows of F become linearly dependent [21]. This results in very large values of the coefficients C of (9) with strong coupling to higher order modes.

To calculate the quality factor of such a resonator, we compare the response to a Fano-resonance [23], which is given by

$$R = \frac{r^2(\omega - \omega_0)^2 + t^2(1/\tau)^2 - 2rt(\omega - \omega_0)(1/\tau)}{(\omega - \omega_0)^2 + (1/\tau)^2} \quad (14a)$$

where ω_0 is the resonant frequency, τ is the resonance lifetime, and r and t are reflectivity and transmittance of a slab of the same thickness as the grating structure being studied. Fano-resonance occurs due to the interference between a narrow-band and broadband scattering phenomenon, which in the case of HCG comes from the transverse higher order harmonic interference with the zero-order mode. The quality factor of the resonator is given as

$$Q = \omega_0\tau. \quad (14b)$$

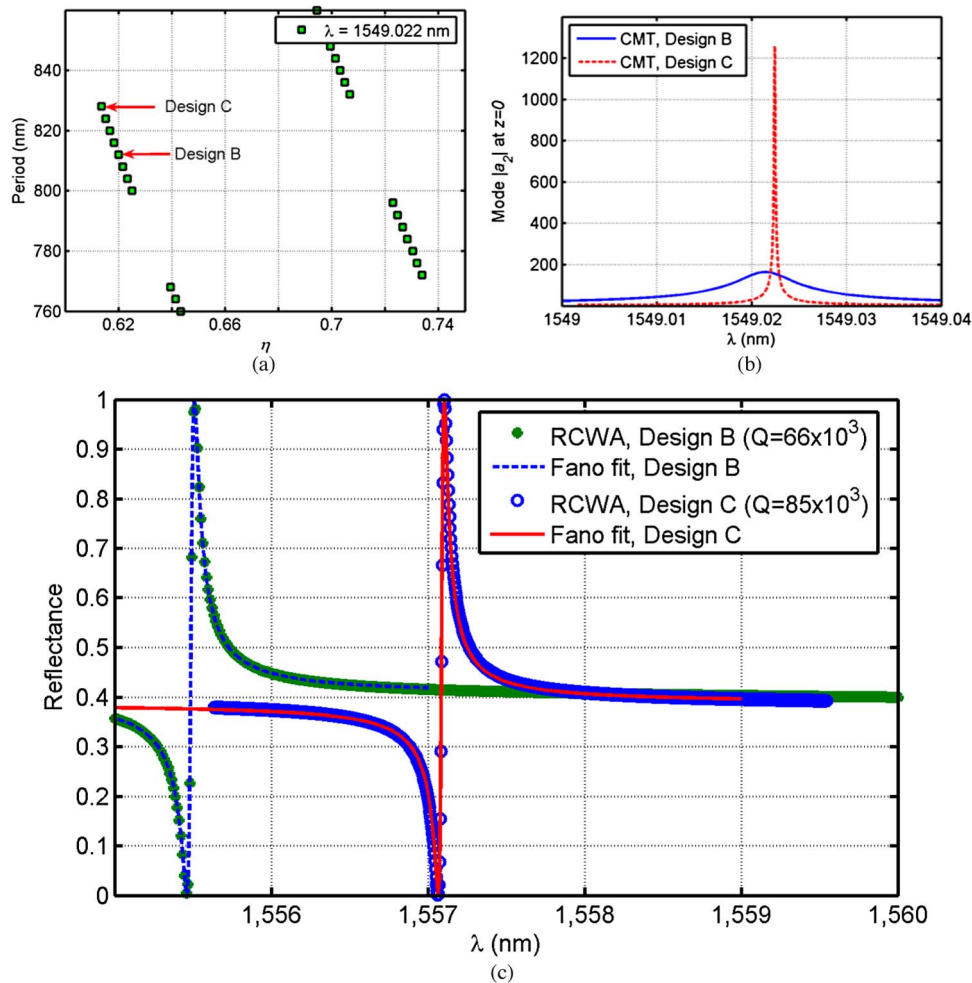


Fig. 5. (a) Maximum field strength of the first higher order mode a_2 versus period Λ and duty cycle η with thickness $d = 625$ nm and grating refractive index of 3.078 using CMT. (b) Comparison of the two designs regarding the strength of interaction between the incident and the evanescent higher order modes. (c) Reflectivity using RCWA with 18 modes. For Design C, $w = 519.68$ nm and $\Lambda = 812$ nm, and for design D, $w = 519.27$ and $\Lambda = 828$ nm. Q values obtained from the fit are 66×10^3 and 85×10^3 for design C and D, respectively.

The stronger the interaction of the incident normal mode with the in-plane higher order harmonics, the narrower the resonance. It should be mentioned here that these narrow-band resonator structures are extremely sensitive to dimensions, and the numerical calculations can require a large number of modes to be accurate.

Fig. 5(a) shows the points of maximum field strength for the first higher order mode a_2 as a function of period and duty cycle of the gratings with a slab thickness of $d = 625$ nm and grating index $n_2 = 3.078$, using the proposed method. Two designs are pointed out for comparison and to demonstrate the strength of the method in finding an improved configuration. Design C with period of 812 nm was proposed previously [22]. Design D results in a Q-factor of 46 times higher than Design C. It should be noted that these values were obtained using only three modes. To obtain full convergence, however, RCWA requires at least 18 modes, as shown in Fig. 5(c). (In this case, RCWA is better suited for the high-quality simulations, which require long simulation times with FDTD; however, close agreement was found with FDTD simulations with a long integration time.) The Fano-fit is also plotted in Fig. 5(c). Q-factor values obtained from the fit are 66×10^3 for Design C and 85×10^3 for Design D. There is a significant reduction in the actual Q factor in the fully

converged case; however, the trend of increase in Q is maintained for the RCWA (as with the CMT method): Going from Design C to D shows an increase of 28% in the Q value. Therefore, the CMT method improves the performance of these high-Q resonators, as well as providing suitable parameters for strong coupling to the first higher order mode.

4. Conclusion

We presented a CMT method to explore the characteristics of HCGs over a wide range of design parameters such as period, duty cycle, thickness, and wavelength of operation. A design procedure was presented for broadband high reflectivity applications that showed near-optimal performance in terms of broadband reflection with minimal ripple. Such broadband reflectors are of interest for numerous applications, including tunable VCSELs. The method was also used to search for higher Q resonators, with a 28% improvement over past results demonstrated. These high-Q resonators are of particular interest for sensor applications. Other desirable features of the CMT method are its efficiency, simplicity, and ability to provide physical insight. It should be mentioned that the method provides estimates for an optimal design, and once the dimensions are estimated for desired operation, RCWA/FDTD or any other rigorous method (including higher order CMT) can be used to accurately describe the optical properties of these structures.

References

- [1] A. W. Snyder and J. D. Love, *Optical Waveguide Theory*. New York: Chapman & Hall, 1983.
- [2] J. R. Pierce, "Coupling of modes of propagation," *J. Appl. Phys.*, vol. 25, no. 2, pp. 179–183, Feb. 1954.
- [3] A. Yariv, "Coupled-mode theory for guided-wave optics," *IEEE J. Quantum Electron.*, vol. QE-9, no. 9, pp. 919–933, Sep. 1973.
- [4] R. A. Waldron, "The theory of coupled modes," *Q. J. Mech. Appl. Math.*, vol. 18, pp. 385–404, 1964.
- [5] W. Huang and J. Mu, "Complex coupled-mode theory for optical waveguides," *Opt. Express*, vol. 17, no. 21, pp. 19 134–19 152, Oct. 2009.
- [6] S. P. Davis, *Diffraction Grating Spectrographs*. New York: Holt, Rinehart and Winston, 1970.
- [7] F. Kneubuhl, "Diffraction grating spectroscopy," *Appl. Opt.*, vol. 8, no. 3, pp. 505–519, 1969.
- [8] G. A. De Biase, F. Sacchetti, and D. Trevese, "Spectroscopy by grating synthesis," *Appl. Opt.*, vol. 11, no. 5, pp. 1163–1168, 1972.
- [9] K. T. V. Grattan and B. T. Meggitt, *Optical Fiber Sensor Technology, Advanced Applications, Bragg Gratings and Distributed Sensors*. Boston, MA: Kluwer, 2000.
- [10] E. G. Loewen and E. Popov, *Diffraction Gratings and Applications*. New York: Marcel Dekker, 1997.
- [11] C. J. Chang-Hasnain, C. L. G. Savran, and A. Cagri, "In situ assembled diffraction grating for biomolecular detection," *Appl. Phys. Lett.*, vol. 90, no. 23, p. 233 901, Jun. 2007.
- [12] A. Haglund, J. S. Gustavsson, J. Bengtsson, and P. Jedrasik, "Design and evaluation of fundamental-mode and polarization-stabilized VCSELs with a subwavelength surface grating," *IEEE J. Quantum Electron.*, vol. 42, no. 3, pp. 231–240, Mar. 2006.
- [13] S. Goeman, S. Boons, B. Dhoedt, K. Vandeputte, K. Caekebeke, P. V. Daele, and R. Baets, "First demonstration of highly reflective and highly polarization selective diffraction gratings (GIRO-gratings) for long-wavelength VCSELs," *IEEE Photon. Technol. Lett.*, vol. 10, no. 9, pp. 1205–1207, Sep. 1998.
- [14] M. Ortsiefer, M. Gorblich, E. Yan Xu, J. Ronneberg, R. Roskopf, and M. C. Shau, "Polarization control in buried tunnel junction VCSELs using a birefringent semiconductor/dielectric subwavelength grating," *IEEE Photon. Technol. Lett.*, vol. 22, no. 1, pp. 15–17, Jan. 2010.
- [15] Y. Kanamori, M. Ishimori, and K. Hane, "High efficient light-emitting diodes with antireflection subwavelength gratings," *IEEE Photon. Technol. Lett.*, vol. 14, no. 8, pp. 1064–1066, Aug. 2002.
- [16] C. F. R. Mateus, M. C. Y. Huang, D. Yunfei, A. R. Neureuther, and C. J. Chang-Hasnain, "Ultrabroadband mirror using low-index cladded subwavelength grating," *IEEE Photon. Technol. Lett.*, vol. 16, no. 2, pp. 518–520, Feb. 2004.
- [17] C. F. R. Mateus, M. C. Y. Huang, C. Lu, C. J. Chang-Hasnain, and Y. Suzuki, "Broad-band mirror (1.12–1.62 μm) using a subwavelength grating," *IEEE Photon. Technol. Lett.*, vol. 16, no. 7, pp. 1676–1678, Jul. 2004.
- [18] M. G. Moharam and T. K. Gaylord, "Rigorous coupled-wave analysis of metallic surface-relief gratings," *J. Opt. Soc. Amer. A, Opt. Image Sci.*, vol. 3, no. 11, pp. 1780–1787, Nov. 1986.
- [19] K. Hwan, L. Chrostowski, E. Bisailon, and D. Plant, "DBR, sub-wavelength grating, and photonic crystal slab Fabry-Pérot cavity design using phase analysis by FDTD," *Opt. Express*, vol. 15, no. 16, pp. 10 330–10 339, Aug. 2007.
- [20] D. M. Whittaker and I. S. Culshaw, "Scattering-matrix treatment of patterned multilayer photonic structures," *Phys. Rev. B, Condens. Matter*, vol. 60, no. 4, pp. 2610–2618, Jul. 1999.
- [21] C. D. Meyer, *Matrix Analysis and Applied Linear Algebra*. Philadelphia, PA: SIAM, 2000.

- [22] Y. Zhou, C. Y. Huang, C. Chase, V. Karagodsky, M. Moewe, B. Pasala, G. Sedgwick, and C. J. Chang-Hasnain, "High-index-contrast grating (HCG) and its applications in optoelectronic devices," *IEEE J. Sel. Topics Quantum Electron.*, vol. 15, no. 5, pp. 1–15, Sep./Oct. 2009.
- [23] S. Fan, W. Suh, and J. D. Joannopoulos, "Temporal coupled-mode theory for the Fano resonance in optical resonators," *J. Opt. Soc. Amer. A, Opt. Image Sci.*, vol. 20, no. 3, pp. 569–572, 2003.
- [24] S. M. Tripathi, A. Kumar, E. Marin, and J.-P. Meunier, "Bragg grating based biochemical sensor using submicron Si/SiO₂ waveguides for lab-on-a-chip applications: A novel design," *Appl. Opt.*, vol. 48, no. 23, pp. 4562–4567, Aug. 2009.